論文 / 著書情報
Article / Book Information

Title	Structure and energetics of carbon defects in SiC (0001)/SiO2 systems at realistic temperatures: Defects in SiC, SiO2, and at their interface
Authors	Takuma Kobayashi, Yu-ichiro Matsushita
Citation	Journal of Applied Physics, Vol. 126, No. 14, p. 145302
Pub. date	2019, 10
Note	This article may be downloaded for personal use only. Any other use requires prior permission of the author and AIP Publishing. This article appeared in Journal of Applied Physics, Vol. 126, No. 14, p. 145302 and may be found at https://doi.org/10.1063/1.5100754.

Journal of Applied Physics ARTICLE scitation.org/journal/jap

Structure and energetics of carbon defects in SiC (0001)/SiO_2 systems at realistic temperatures: Defects in SiC, SiO_2, and at their interface

Cite as: J. Appl. Phys. **126**, 145302 (2019); doi: 10.1063/1.5100754
Submitted: 25 April 2019 · Accepted: 25 September 2019 ·
Published Online: 10 October 2019

Takuma Kobayashi[a] and Yu-ichiro Matsushita

AFFILIATIONS

Laboratory for Materials and Structures, Institute of Innovative Research, Tokyo Institute of Technology, Yokohama 226-8503, Japan

[a]kobayashi.t.cp@msl.titech.ac.jp

ABSTRACT

We report systematic first-principles calculations that reveal the atomic configurations, stability, and energy levels of carbon defects in SiC (0001)/SiO_2 systems. We clarify the stable position (i.e., in SiC, SiO_2, or at SiC/SiO_2 interfaces) of defects depending on the oxidation environment (an oxygen-rich or -poor condition). At finite temperatures, the chemical potential of atomic species was corrected referring to thermochemical tables in order to obtain the temperature-dependent defect formation energies. Under an oxygen-rich condition, we found that the dicarbon antisite $[(C_2)_{Si}]$ in SiC is one of the favorable defects at a typical oxidation temperature of 1600 K and it creates a localized level near the conduction band edge of SiC, being a critical defect for *n*-channel metal-oxide-semiconductor field-effect transistors (MOSFETs). A variety of carbon-dimer defects at a SiC/SiO_2 interface, such as Si—CO—CO_2, Si—CO—CO—Si, and Si—(CO)—CO_2, are stable under the oxygen-rich condition at 1600 K, and they create localized levels relatively close to the valence band edge of SiC, thus being critical defects for *p*-channel MOSFETs. In the viewpoint of static energetics, our results suggest that the oxidation of SiC under a high-temperature oxygen-poor condition is effective in suppressing the generation of carbon defects.

I. INTRODUCTION

Silicon carbide (SiC) has attracted increasing attention as a suitable material for next-generation power devices, owing to its superior physical properties (e.g., wide bandgap, high critical electric field, high electron saturation velocity, and high thermal conductivity).[1,2] One of the unique advantages of SiC over other compound semiconductors is that it can be thermally oxidized to form silicon dioxide (SiO_2). Thus, SiC metal-oxide-semiconductor field-effect transistors (MOSFETs) have been recognized as a strong candidate for power switching devices.[1,2]

Despite their promising characteristics for applications, SiC MOSFETs have suffered from the unexpectedly low channel mobility, which is certainly due to the high interface state density (D_{IT}) of SiC/SiO_2 systems ($\sim 10^{13}\,eV^{-1}\,cm^{-2}$).[2–7] Due to this high D_{IT}, which is a thousandfold higher than that in typical silicon (Si)/SiO_2 systems ($\sim 10^{10}\,eV^{-1}\,cm^{-2}$),[8] the field-effect mobility of SiC MOSFETs is mainly limited by the carrier trapping effect of the interface states, even after proper interface nitridation.[7]

Although the microscopic origin of the interface states is not yet identified, carbon defects have been widely believed as a possible origin. Indeed, a study based on internal photoemission (IPE) spectroscopy suggested the existence of sp^2-bonded and graphite-like carbon clusters near a SiC/SiO_2 interface.[9] A report based on secondary ion mass spectrometry (SIMS) also provided evidence of carbon defects and discussed the correlation between the interface quality and the excess carbon density.[10] Besides, a signal originating from carbon dangling bonds at a SiC/SiO_2 interface was detected by utilizing electron-spin-resonance (ESR) spectrometry.[11]

Theoretical calculations also suggested various candidates of carbon defects so far.[12–22] As a few examples, dicarbon antisites $[(C_2)_{Si}]$[12,13] in SiC, Si_2—C—O[14] and Si_2—C═C—Si_2[15–17] structures in SiO_2, and Si—(CO)—Si defects[12] at a SiC/SiO_2 interface have been suggested. There is also a report that even larger carbon clusters are possible to exist near the interface.[13,15] Meanwhile, it was suggested that the interface states might originate from the irregularities of SiC at the interface (i.e., not atomically smooth surface).[23]

However, very few of the previous reports systematically deal with the defects in SiC and SiO_2 and at SiC/SiO_2 interfaces.

In the present study, we, therefore, perform systematic first-principles calculations that reveal the stable atomic configurations of carbon defects in SiC, SiO_2, and at SiC/SiO_2 interfaces. We investigated 114 types of possible defect configurations and compared their formation energies under certain chemical potential conditions to discuss their stability depending on the oxidation environment (an O-rich or -poor condition). The temperature dependence of defect formation energies was also obtained by correcting the chemical potentials of atomic species at finite temperatures by referring to the NIST-JANAF thermochemical tables.[24] We also calculate the localized levels induced by the defects which are relatively stable at a typical oxidation temperature of SiC.

II. CALCULATION CONDITIONS

A. Computational methodologies

All the calculations in this study were carried out on the basis of density functional theory (DFT)[25,26] by using the Vienna *ab initio* simulation package (VASP).[27,28] Both the structural optimization and the calculation of one-electron energy levels were performed by using the Heyd-Scuseria-Ernzerhof (HSE06) hybrid functional[29–31] to reproduce the experimental bandgap of SiC well. The projector augmented wave (PAW) method[32] as implemented in the VASP code was applied in the calculations. The cutoff energy was set to 400 eV in the plane-wave basis set, and the structural optimization was performed until the remaining forces of the structures became less than 40 meV $Å^{-1}$. A single k-point (the Γ point) was sampled for the overall calculations.

B. Modeling of defects

We used a 128-atom 4H-SiC supercell (a $4 \times 4 \times 1$ supercell), a 72-atom α-quartz SiO_2 supercell, and a 224-atom 4H-SiC surface slab to investigate the carbon defects in SiC, SiO_2, and at their interface, respectively. We considered 114 types of defect configurations (23, 12, and 79 types of defects in SiC, SiO_2, and at a SiC/SiO_2 interface, respectively) to investigate a variety of mono- and dicarbon defects. In investigating the carbon defects in SiC, we introduced one or two additional C atoms into the 4H-SiC supercell (Fig. 1) at the positions described in Fig. 2 (i.e., a, b, a', b', 1, 2, 3, 4, 1', 2', 3', and 4') with and without removing Si atoms, and performed structural optimization to obtain the stable defect configurations. For instance, if we introduce a C atom into the position a in Fig. 2, we obtain a C-on-Si antisite (C_{Si}). For defects in SiO_2, we focused on the dicarbon defects which are reported to be stable (or metastable) from previous first-principles molecular dynamics (MD) calculations.[16] In the 72-atom α-quartz SiO_2 supercell (Fig. 3), we reproduced the reported defect configurations shown in Fig. 4 and optimized them to obtain stable defect configurations.

In investigating the defects at a SiC (0001)/SiO_2 interface, we prepared a 224-atom 4H-SiC surface slab of which surface atoms were terminated by H atoms, as shown in Fig. 5. The H atoms at the (0001) face were inserted to remove the dangling bonds of surface Si atoms, which are supposed to be attached to O atoms of amorphous SiO_2 in SiC (0001)/SiO_2 systems. The surface C atoms at the $(000\bar{1})$ face should be connected to bulk SiC, which were also terminated by H atoms. We adopted this surface-slab model instead of preparing SiC (0001)/amorphous-SiO_2 systems in investigating the defects, to eliminate the energy cost for the surrounding amorphous-SiO_2 structure which depends on each specimen (i.e., each defect configuration) and to compare the formation energies of carbon defects on equal footing. In more detail, if a defect is introduced at the SiC/amorphous-SiO_2 interface and then its geometry is optimized, the total energy of the system will substantially be affected by the local distortion of amorphous-SiO_2 structure around the defect. Since such a distortion will be released in the realistic situation, we adopted a surface-slab model to avoid this problem. We confirmed that the calculated bandgap is sufficiently

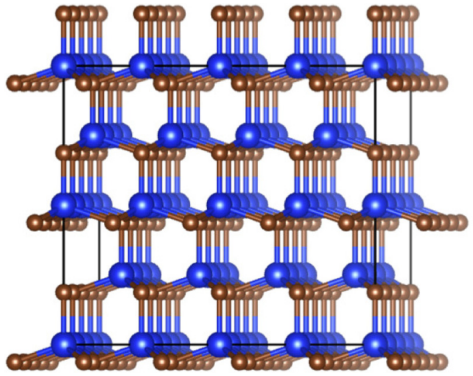

FIG. 1. 128-atom 4H-SiC supercell (a $4 \times 4 \times 1$ supercell) used to investigate the carbon defects in the present study. The blue and brown balls indicate the Si and C atoms, respectively.

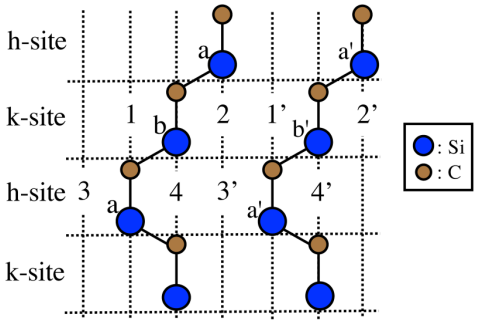

FIG. 2. Positions to introduce carbon atoms in 4H-SiC. Positions a, b, a', and b' are the Si-sites, and positions 1, 2, 3, 4, 1', 2', 3', and 4' are the interstitial sites. Note that sites a', b', 1', 2', 3', and 4' are equivalent to sites a, b, 1, 2, 3, and 4, respectively, but are labeled to describe the defect pair combinations. We investigated single antisites (a and b), single interstitials (1–4), antisite-antisite pairs [(a, b), (a, a'), (b, b')], antisite-interstitial pairs [(a, 2), (a, 3), (a, 4), (b, 1), (b, 2), and (b, 4)], and interstitial-interstitial pairs [(1, 2), (1, 3), (1, 4), (2, 3), (2, 4), (3, 4), (2, 1'), and (4, 3')] in the present study.

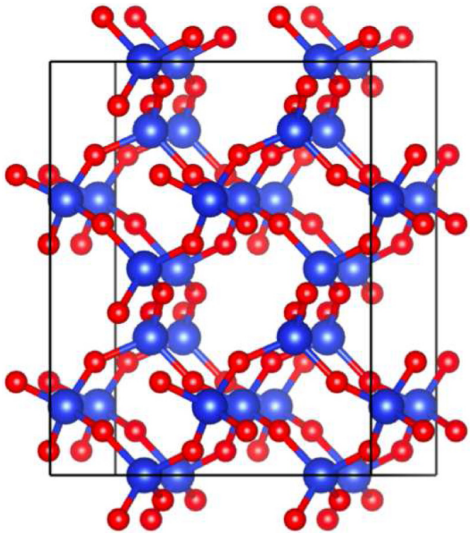

FIG. 3. 72-atom α-quartz SiO_2 supercell used to investigate the carbon defects in the present study. The blue and red balls indicate the Si and O atoms, respectively.

converged with respect to the slab thickness and is also close to the experimental value of 3.26 eV at 300 K;[2] the calculated bandgap was 3.39 eV and 3.36 eV for 224- and 256-atom slabs, respectively. In investigating the defects, carbon atoms were inserted on the top of the surface Si atoms at a SiC (0001) surface with removing several H atoms from the surface. The investigated defect configurations are depicted in Fig. 6. In preparing the c1d1 defects in Fig. 6, for instance, we put a single C atom above the center of gravity of three topmost Si atoms, together with removing three surface H atoms. Then, three C—Si bonds are generated. A dangling bond is left on the inserted C atom, which is treated by four different ways, as depicted in Fig. 7; a dangling bond (d), O— (o), OH— (h), and SiH_3— (s) terminations. Finally, structural optimization is performed to obtain stable defect configurations.

C. Defect formation energy

The formation energy, E_F, of a neutral defect was calculated by

$$E_F = E_D - E_0 - \sum_i N_i \mu_i, \tag{1}$$

where E_D and E_0 are the total energies of the simulation cell with and without the defect, respectively. N_i and μ_i are the number of the removed ($N_i < 0$) or added ($N_i > 0$) i-type atoms and its chemical potential, respectively. We supposed four extreme situations, where the chemical potentials of the atomic species were calculated as

$$\begin{aligned} &\mu_{Si} = E(SiO_2) - 2\mu_O, \quad \mu_C = E(SiC) - \mu_{Si}, \\ &\mu_O = \frac{E(O_2)}{2} \quad \text{(C-rich, O-rich);} \end{aligned} \tag{2}$$

$$\begin{aligned} &\mu_{Si} = E(Si), \quad \mu_C = E(CO_2) - 2\mu_O, \\ &\mu_O = \frac{E(SiO_2) - \mu_{Si}}{2} \quad \text{(C-rich, O-rich);} \end{aligned} \tag{3}$$

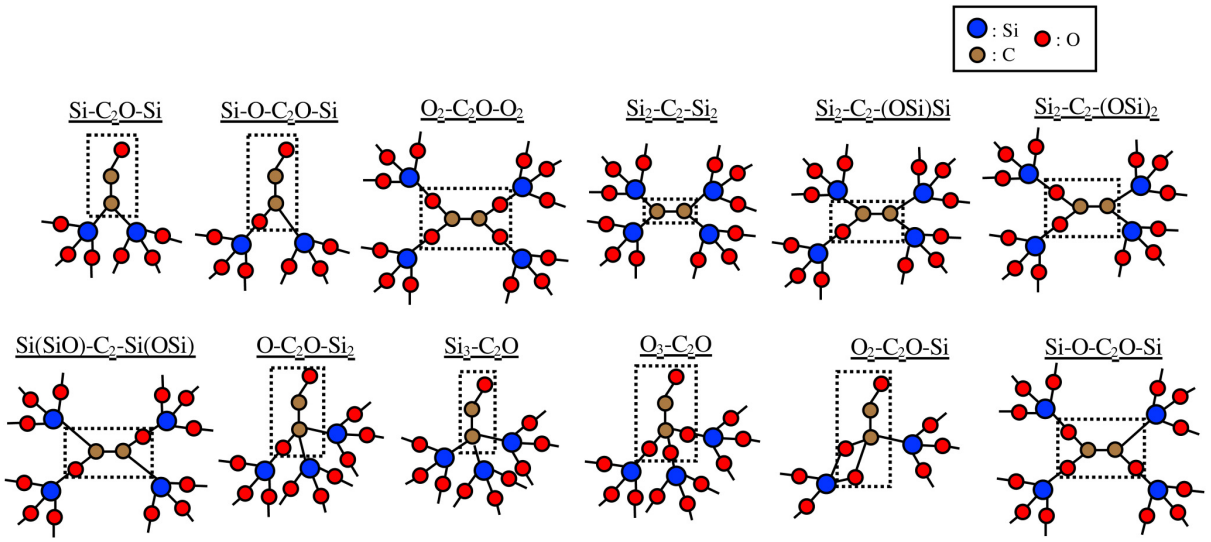

FIG. 4. Structure of carbon defects in SiO_2 investigated in the present study. The defects were selected on the basis of the results of first-principles molecular dynamics (MD) calculations.[16]

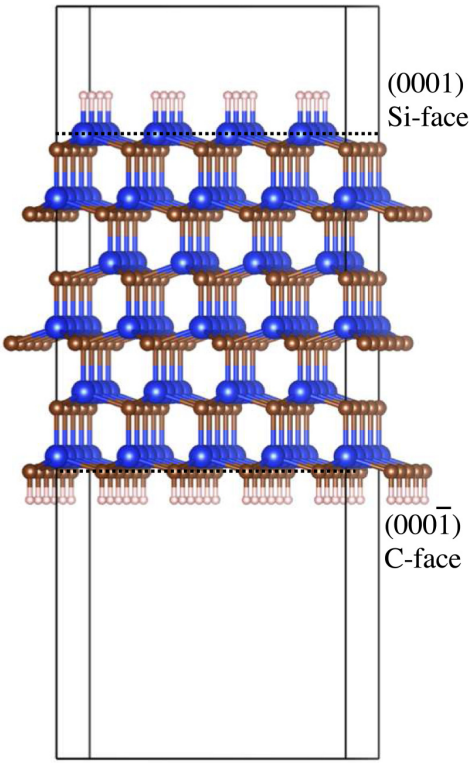

FIG. 5. 224-atom 4H-SiC surface slab prepared in order to investigate the carbon defects at a SiC/SiO_2 interface. The surface Si and C atoms are terminated by H atoms. The blue, brown, and small white balls are the Si, C, and H atoms, respectively. The slab and vacuum thicknesses are 15.7 and 13.6 Å, respectively.

$$\mu_{Si} = E(SiO_2) - 2\mu_O, \quad \mu_C = E(CO_2) - 2\mu_O, \quad \mu_O = \frac{E(O_2)}{2} \ \text{(C-rich, O-rich)}; \tag{4}$$

$$\mu_{Si} = E(Si), \quad \mu_C = E(SiC) - \mu_{Si}, \quad \mu_O = \frac{E(SiO_2) - \mu_{Si}}{2} \ \text{(C-rich, O-rich)}. \tag{5}$$

Here, $E(Si)$, $E(CO_2)$, $E(SiO_2)$, $E(O_2)$, and $E(SiC)$ are the total energies of crystal silicon (Si), a carbon dioxide (CO_2) molecule, α-quartz SiO_2, an oxygen (O_2) molecule, and 4H-SiC per formula unit, respectively. The calculated values of $E(Si)$, $E(CO_2)$, $E(SiO_2)$, $E(O_2)$, and $E(SiC)$ were −6.28, −28.33, −29.16, −13.96, and −17.43 eV, respectively, at 0 K. We derived the relationships among the chemical potentials [Eqs. (2)–(5)] as follows: first, we assumed chemical equilibrium among Si, O_2, and SiO_2 during the oxidation of SiC and considered the O-rich or -poor condition, where μ_{Si} and μ_O were calculated as $\mu_{Si} = E(SiO_2) - 2\mu_O$ and $\mu_O = E(O_2)/2$ (O-rich) or $\mu_{Si} = E(Si)$ and $\mu_O = (E(SiO_2) - \mu_{Si})/2$ (O-poor). Then, μ_C was calculated either by $\mu_C = E(SiC) - \mu_{Si}$ or $\mu_C = E(CO_2) - 2\mu_O$, depending on the condition (O-rich or O-poor). Since the chemical potential of Si is low (−15.19 eV) and that of O is high (−6.98 eV) under the O-rich condition, $\mu_C = E(SiC) - \mu_{Si}$ (= −2.23 eV) and $\mu_C = E(CO_2) - 2\mu_O$ (= −14.37 eV) correspond to the C-rich and -poor limits, respectively. Conversely, under the O-poor condition, since the chemical potential of Si is high (−6.28 eV) and that of O is low (−11.44 eV), $\mu_C = E(SiC) - \mu_{Si}$ (= −11.15 eV) and $\mu_C = E(CO_2) - 2\mu_O$ (= −5.45 eV) correspond to the C-poor and -rich limits, respectively. As we focused on the carbon defects, we considered the C-rich limits [Eqs. (2) and (3)] in the present study. Note that, in these extreme carbon-rich conditions [Eq. (2) and (3)], μ_C takes even higher values than that in diamond (i.e., $\mu_C = E(C) = -10.52$ eV). As we approximated the SiC/SiO_2 interface with an H-terminated SiC slab (Fig. 5), the chemical potential of an H atom is also needed to calculate the formation energy [Eq. (1)], which was calculated as

$$\mu_H = \frac{E(SiH_4) - \mu_{Si}}{4}, \tag{6}$$

irrespective of the conditions [Eq. (2) or (3)]. Here, $E(SiH_4)$ is the total energy of a silane (SiH_4) molecule per formula unit; the calculated value of $E(SiH_4)$ was −21.95 eV at 0 K. Since most of the H atoms were used to terminate the Si-dangling bonds, we here adopted $E(SiH_4)$ in calculating μ_H. At finite temperatures, we obtained the temperature dependence of enthalpy, $H(T)$ and entropy, $S(T)$ of gaseous molecules, O_2, CO, CO_2, and SiH_4 at the standard state pressure ($p^0 = 0.1$ MPa) from the NIST-JANAF thermochemical tables[24] to correct their energies.

III. RESULTS AND DISCUSSION

A. Defect formation energy

Figures 8(a) and 8(b) show the temperature dependence of formation energies for the carbon defects in SiC (0001)/SiO_2 systems. Here, the energies of gaseous CO and CO_2 molecules are also shown for comparison. The structure of the carbon defects is depicted in Fig. 9. Since a C-rich situation is considered, dicarbon defects tend to be more favorable than the monocarbon ones at either condition (O-rich or -poor), as shown in Fig. 9. At the O-rich limit [Fig. 8(a)], the formation energies of defects #1–#5 are quite low at 1600 K, which is about the typical experimental temperature of SiC oxidation, and the energies are even comparable with those of gaseous CO and CO_2 molecules. Such a result suggests that, during the oxidation of SiC under a condition close to the O-rich limit, a significant portion of C atoms will favor staying around the interface to create defects than to be ejected from the system as CO or CO_2 molecules. We also see that the defects with O atoms tend to appear as stable forms in the O-rich condition (Fig. 9). At the O-poor limit [Fig. 8(b)], the formation energies of the defects are relatively high compared to the energies of CO and CO_2 molecules. Therefore, in the viewpoint of static energetics, oxidation under an O-poor condition is more favorable than under

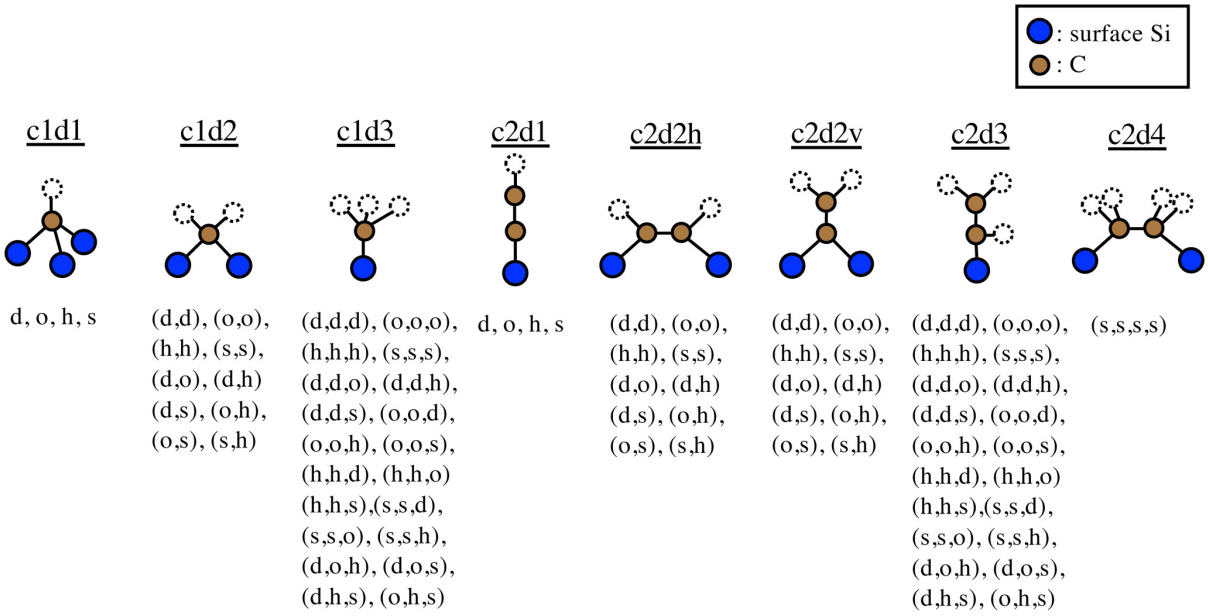

FIG. 6. Structure of carbon defects at a SiC (0001)/SiO_2 interface investigated in the present study. The dangling bonds (depicted by dotted circles) of each structure were treated by four different ways as described in Fig. 7. The investigated defect configurations are indicated by the combination of alphabets; for instance, for the c1d2 defects, we treated the two dangling bonds of the inserted C atom by 10 types of combinations of termination; (d, d), (o, o), (h, h), (s, s), (d, o), (d, h), (d, s), (o, h), (o, s), and (s, h).

an O-rich condition in reducing the carbon defects at a SiC/SiO_2 interface. When looking at the temperature dependences, CO and CO_2 molecules become more favorable compared to the carbon defects at higher temperatures, suggesting that oxidation at higher temperatures is also favorable. In fact, a recent experimental study proved that high-temperature oxidation over 1400 °C (~1670 K) combined with rapid cooling reduces the defects at a SiC (0001)/SiO_2 interface.[33] Also, post-oxidation annealing in argon (Ar) ambient with a very low oxygen partial pressure at 1500 °C (~1770 K), of which condition is considered to be close to the O-poor limit [Fig. 8(b)], reduces defects at SiC (0001)/SiO_2 interfaces.[34] Such results can be qualitatively understood by our calculation results.

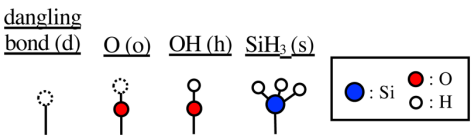

FIG. 7. Four ways to treat each dangling bond of carbon atoms in Fig. 6; a dangling bond (d), O— (o), OH— (h), and SiH_3— (s) terminations. Note that the structures were attached to H atoms instead of Si or O atoms of amorphous SiO_2.

B. Defect energy levels

Figure 10 shows the energy levels of the carbon defects stable at 1600 K under either the O-rich or -poor condition. Under the O-rich condition, the dicarbon antisite in the SiC side [$(C_2)_{Si}$ (#2)] is stable (Fig. 9), and it creates a defect level near the conduction band edge (E_C) of SiC (about E_C−0.1 eV for the h-site and E_C−0.4 eV for the k-site defect: Fig. 10),[35] thus being a critical defect for *n*-channel MOSFETs. Under the O-rich condition [Eq. (2)], the chemical potential of Si is low (Si-poor) and that of C is high (C-rich), which facilitates the creation of $(C_2)_{Si}$ by lowering the formation energies of silicon vacancies and carbon clusters at the same time. The existence of $(C_2)_{Si}$ near the SiC/SiO_2 interface is also predicted in Refs. 12 and 13, where models with top-SiO_2 layers were employed. Many types of interface carbon-dimer defects, such as Si—CO—CO_2 (#1), Si—CO—CO—Si (#4), and Si—(CO)—CO_2 (#5), are stable under the O-rich condition and they create defect levels relatively close to the valence band edge (E_V) of SiC (Fig. 10). Thus, they are critical defects for *p*-channel MOSFETs. For the O-poor condition, the interface carbon-dimer defect (Si—C—C—Si, #6) is the most stable and it will affect the performance of *n*-channel MOSFETs, since it creates a defect level near E_C (about E_C−0.1 eV: Fig. 10). We see that the carbon-dimer defect in the SiO_2 side (Si_2—C—C—Si_2, #9) appears as one of the metastable defects, which is also discussed in previous literature.[16,17] For *p*-channel MOSFETs, the O-poor condition seems to

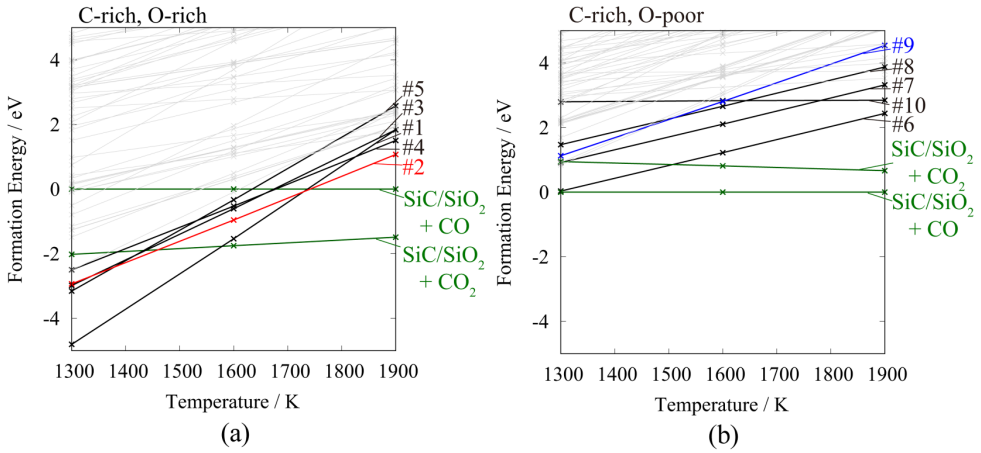

FIG. 8. Temperature dependence of defect formation energies in comparison with the energies of gaseous CO and CO_2 molecules at the (a) C-rich, O-rich and (b) C-rich, O-poor limits. The zeros of the formation energies are set at the energy of a CO molecule. The structure of the defects (#1–#10) is depicted in Fig. 9. The temperature dependence of defect formation energies was calculated by correcting the chemical potentials of atomic species at finite temperatures by referring to thermochemical tables[24] as described in Sec. II C. Lines in dark contrast (red, blue, and black) indicate the defects stable at 1600 K, which is about the typical experimental temperature of SiC oxidation. The red, blue, and black solid lines correspond to the energies of defects in SiC, SiO_2, and at SiC/SiO_2 interfaces, respectively. Green lines represent the energies of gaseous CO and CO_2 molecules.

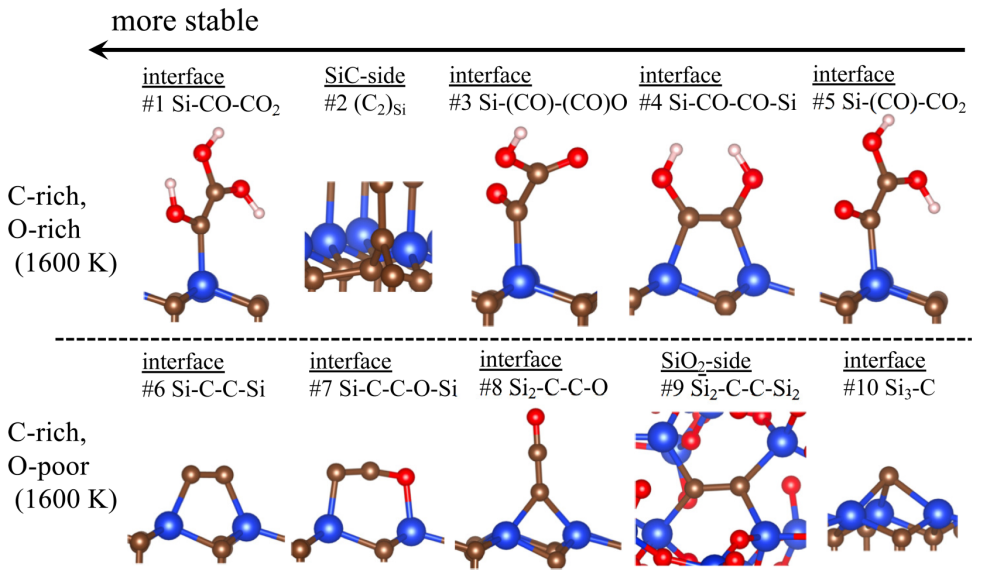

FIG. 9. Structure of the defects stable at 1600 K, which is about the typical experimental temperature of SiC oxidation. The structures are listed in order of stability in either oxidation environment (the C-rich, O-rich or C-rich, O-poor limit). The blue, brown, red, and small white balls are the Si, C, O, and H atoms, respectively. Note that the structures were attached to H atoms instead of Si or O atoms of amorphous SiO_2.

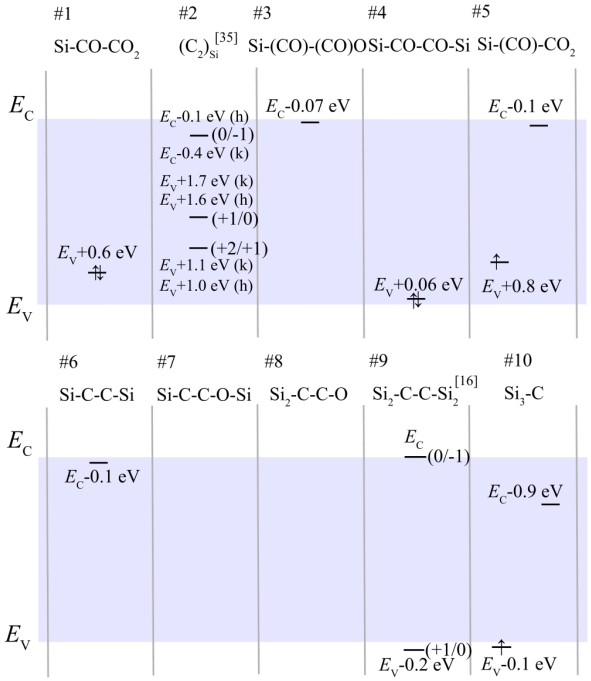

FIG. 10. Calculated electron energy levels for the carbon defects depicted in Fig. 9. E_C and E_V are the conduction and valence band edges of 4H-SiC, respectively, and the light purple area represents the forbidden gap region of 4H-SiC. The charge transition levels for defects in SiC (#2) and in SiO_2 (#9) are taken from Refs. 35 and 16, respectively. The results for both h- and k-site defects are shown for the defect in SiC (#2). For the one-electron energy levels (#1, #3–#6, and #10), the ground-state spin configurations are also indicated.

be quite favorable, and there are few stable defects which create defect levels near E_V inside the bandgap (Figs. 9 and 10).

IV. SUMMARY

We investigated the stable atomic configurations and energy levels of carbon defects in SiC and SiO_2, and at SiC (0001)/SiO_2 interfaces. The temperature-dependent defect formation energies were obtained by correcting the chemical potentials of atomic species at finite temperatures by referring to thermochemical tables. Our results indicate that the oxidation of SiC under an O-rich condition, especially at low temperatures, results in the creation of critical defects for both *n*- and *p*-channel MOSFETs. For instance, the dicarbon antisite in the SiC side [$(C_2)_{Si}$ (#2)] is stable under the O-rich condition, and it creates a defect level near E_C, being crucial for *n*-channel MOSFETs. As critical defects for *p*-channel MOSFETs, many types of interface carbon-dimer defects, such as Si—CO—CO_2 (#1), Si—CO—CO—Si (#4), and Si—(CO)—CO_2 (#5), are stable under the O-rich condition and they create defect levels relatively close to E_V. Thus, in the viewpoint of static energetics, we suggest the oxidation of SiC at a high-temperature O-poor condition in order to suppress the generation of the carbon defects.

ACKNOWLEDGMENTS

Computations were performed mainly at the Center for Computational Science, University of Tsukuba, and the Supercomputer Center at the Institute for Solid State Physics, The University of Tokyo. The authors acknowledge the support from the JSPS Grant-in-Aid for Scientific Research (A) (Grant Nos. 18H03770 and 18H03873).

REFERENCES

[1]B. J. Baliga, IEEE Electron Device Lett. **10**, 455 (1989).
[2]T. Kimoto and J. A. Cooper, *Fundamentals of Silicon Carbide Technology* (Wiley, Singapore, 2014).
[3]N. S. Saks, S. S. Mani, and A. K. Agarwal, Appl. Phys. Lett. **76**, 2250 (2000).
[4]H. Yoshioka, J. Senzaki, A. Shimozato, Y. Tanaka, and H. Okumura, AIP Adv. **5**, 017109 (2015).
[5]M. Noborio, J. Suda, S. Beljakowa, M. Krieger, and T. Kimoto, Phys. Status Solidi A **206**, 2374 (2009).
[6]T. P. Chow, H. Naik, and Z. Li, Phys. Status Solidi A **206**, 2478 (2009).
[7]T. Hatakeyama, Y. Kiuchi, M. Sometani, S. Harada, D. Okamoto, H. Yano, Y. Yonezawa, and H. Okumura, Appl. Phys. Express **10**, 046601 (2017).
[8]E. H. Nicollian and J. R. Brews, *MOS Physics and Technology* (John Wiley & Sons, Inc, New York, 1982).
[9]V. V. Afanasev, M. Bassler, G. Pensl, and M. Schulz, Phys. Status Solidi A **162**, 321 (1997).
[10]T. Kobayashi and T. Kimoto, Appl. Phys. Lett. **111**, 062101 (2017).
[11]T. Umeda, G.-W. Kim, T. Okuda, M. Sometani, T. Kimoto, and S. Harada, Appl. Phys. Lett. **113**, 061605 (2018).
[12]S. Wang, S. Dhar, S. Wang, A. C. Ahyi, A. Franceschetti, J. R. Williams, L. C. Feldman, and S. T. Pantelides, Phys. Rev. Lett. **98**, 026101 (2007).
[13]J. M. Knaup, P. Deák, T. Frauenheim, A. Gali, Z. Hajnal, and W. J. Choyke, Phys. Rev. B **71**, 235321 (2005).
[14]F. Devynck, A. Alkauskas, P. Broqvist, and A. Pasquarello, Phys. Rev. B **84**, 235320 (2011).
[15]P. Deák, J. M. Knaup, T. Hornos, C. Thill, A. Gali, and T. Frauenheim, J. Phys. D Appl. Phys. **40**, 6242 (2007).
[16]Y. Matsushita and A. Oshiyama, Jpn. J. Appl. Phys. **57**, 125701 (2018).
[17]N. Tajima, T. Kaneko, T. Yamasaki, J. Nara, T. Schimizu, K. Kato, and T. Ohno, Jpn. J. Appl. Phys. **57**, 04FR09 (2018).
[18]J. M. Knaup, P. Deák, Th. Frauenheim, A. Gali, Z. Hajnal, and W. J. Choyke, Phys. Rev. B **72**, 115323 (2005).
[19]K. Chokawa, S. Kato, K. Kamaiya, and K. Shiraishi, Mater. Sci. Forum **740-742**, 469 (2013).
[20]K. Shiraishi, K. Chokawa, H. Shirakawa, K. Endo, M. Araidai, K. Kamiya, and H. Watanabe, IEDM Tech. Dig. **2014**, 538 (2014).
[21]A. Gavrikov, A. Knizhnik, A. Safonov, A. Scherbinin, A. Bagatur'yants, B. Potapkin, A. Chatterjee, and K. Matocha, J. Appl. Phys. **104**, 093508 (2008).
[22]S. Wang, M. Di Ventra, S. G. Kim, and S. T. Pantelides, Phys. Rev. Lett. **86**, 5946 (2001).
[23]Y. Matsushita and A. Oshiyama, Nano Lett. **17**, 6458 (2017).
[24]NIST-JANAF Thermochemical Tables [https://janaf.nist.gov/].
[25]P. Hohenberg and W. Kohn, Phys. Rev. **136**, B864 (1964).
[26]W. Kohn and L. J. Sham, Phys. Rev. **140**, A1133 (1965).
[27]G. Kresse and J. Furthmüller, Phys. Rev. B **54**, 11169 (1996).
[28]G. Kresse and D. Joubert, Phys. Rev. B **59**, 1758 (1999).
[29]J. Heyd, G. E. Scuseria, and M. Ernzerhof, J. Chem. Phys. **118**, 8207 (2003). [Erratum 124, 219906 (2006)].
[30]J. Paier, M. Marsman, K. Hummer, G. Kresse, I. C. Gerber, and J. G. Ángyán, J. Chem. Phys. **124**, 154709 (2006).

[31]Y. Matsushita, K. Nakamura, and A. Oshiyama, Phys. Rev. B **84**, 075205 (2011).
[32]P. E. Blöchl, Phys. Rev. B **50**, 17953 (1994).
[33]T. Hosoi, D. Nagai, M. Sometani, Y. Katsu, H. Takeda, T. Shimura, M. Takei, and H. Watanabe, Appl. Phys. Lett. **109**, 182114 (2016).
[34]T. Kobayashi, K. Tachiki, K. Ito, and T. Kimoto, Appl. Phys. Express **12**, 031001 (2019).
[35]T. Kobayashi, K. Harada, Y. Kumagai, F. Oba, and Y. Matsushita, J. Appl. Phys. **125**, 125701 (2019).